Surface & Coatings Technology 473 (2023) 129931

Contents lists available at ScienceDirect

Surface & Coatings Technology

journal homepage: www.elsevier.com/locate/surfcoat

Full Length Article

Analysis of electrical resistance measurements as a potential determination method for coating thickness on powders

David Böhm [a,*], Matija Kusztrich [a], Robin Kurinjimala [a], Andreas Eder [b], Christoph Eisenmenger-Sittner [a,*]

[a] Institute of Solid State Physics, TU Wien, Wiedner Hauptstraße 8-10, Vienna, A-1040, Vienna, Austria
[b] MIBA High Tech Coatings GmbH, Dr.-Mitterbauer-Str. 3, Vorchdorf, A-4655, Upper Austria, Austria

ARTICLE INFO

Keywords:
PVD
Magnetron sputtering
Thin films
Metal coatings
Oxide coatings
Powders
Electrical resistance

ABSTRACT

The electrical resistance of conductive and non-conductive coatings on non-conductive and conductive powders, respectively, is investigated under increasing external load. A specially designed equipment was used to deposit coatings on small and light as well as heavy powdery substances by DC magnetron sputtering. Several reference methods to predict or measure the absolute film thickness on powders are discussed.

When measuring the electrical resistance of insulating powders coated with a metal, in this case hollow glass microspheres (HGMs) coated with copper, under increasing load, a typical resistance curve is found. This resistance curve is discussed in terms of percolation theory and the Heckel equation for powder compaction. The influence of coating thickness of the conductive coating is then evaluated and other factors like inhomogeneity of the coating are discussed. To reduce the influence of measurement parameters, selected experiments are interpreted under the concept of a force per grain, which is introduced and explained.

To further substantiate the typical electrical resistance curve, stabilized and non-stabilized NMC811 powder is coated with aluminium and zirconium oxides of different thicknesses, corresponding to a conductive powder with an insulating coating. When comparing measurements for stabilized and non-stabilized powder, the perspective for electrical resistance measurements under increasing load becomes apparent, as it is possible to even detect surface modifications which are not known a priori.

1. Introduction

Magnetron sputtering is a widely used and versatile method for improving and modifying surface and interface properties by the deposition of a thin film [1]. As recent articles have shown, it is not only possible to coat flat surfaces, but also the large effective surface area of a powder bed [2–5].

Therefore, the coating of granulates has gained considerable attention in the fields of powder metallurgy [6] to enhance mechanical properties of sintered parts [7,8] or to increase the oxidation resistance during storage and handling of the powder [9]. Particle size and shape, surface roughness and interactions have a great influence on the flowability and frictional behaviour of powders [10,11]. Thus, modifying the surface of the granulate may improve the flowability and reduce the frictional charge which creates surface cohesion due to Van der Waals interaction [9].

In contrast to the heavy powders used in metallurgy and batteries, solid or hollow glass microspheres (SGMs or HGMs) can be used in a certain range of energy technologies [12]. At a lower technological level, coated HGMs can be used for thermal insulation [13,14], but more sophisticated coatings such as HGMs coated with thermochromic materials [15] are also conceivable. At a higher technological level, hollow glass and polymer microspheres have potential in e.g. hydrogen storage [16] or inertial confinement fusion (ICF) [17].

There is a great interest in the surface modification of powders, not only in the field of powder metallurgy, but also in energy applications. For example, lithium-ion batteries have a large field of applications, ranging from accumulators in electromobility [18] to grid stabilizers in highly fluctuating power grids [19]. Known weak points of the cathode material in batteries are discussed in [20–22]. Oxide surface coatings can improve chemical inertness and mechanical stability, but in return also reduce the rate of Li release [23–26].

* Corresponding authors.
E-mail addresses: david.boehm@tuwien.ac.at (D. Böhm), christoph.eisenmenger@ifp.tuwien.ac.at (C. Eisenmenger-Sittner).

https://doi.org/10.1016/j.surfcoat.2023.129931
Received 25 May 2023; Received in revised form 14 August 2023; Accepted 16 August 2023
Available online 22 August 2023

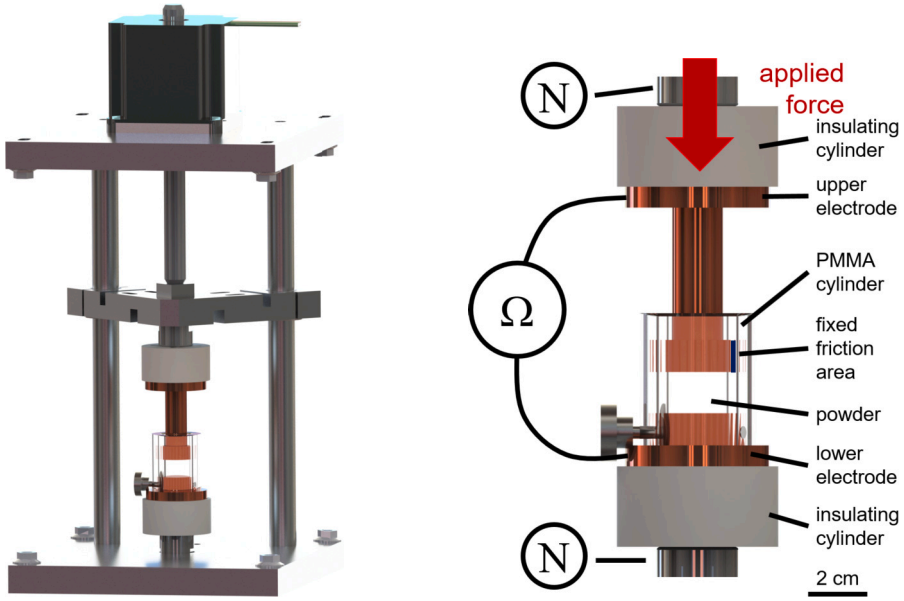

(a) Guided and motorized resistance measurement (b) Detailed model of cylinder and electrodes with description

Fig. 1. 3D-model of the resistance measurement system. (a) Overview with motor and guiding rails and (b) detailed powder cylinder and t-shaped electrode to ensure a fixed area of friction between electrode and cylinder.

On flat surfaces the determination of the film thickness is a relatively easy task. In contrast, for a coated powder, determining the layer thickness is a major challenge. Known methods for layer thickness determination on granulates utilize gravimetry [3], optics in case of a transparent substrate [27,3], electron microscopy [28,5] or focused ion beam (FIB) [5] cross sectional techniques.

In this work, the behaviour of the electrical resistance of coated powders under increasing, external load is investigated. The aim is to find a fast and inexpensive method to determine the presence and, ideally, the thickness of a coating. If other factors are found to affect the electrical resistance measurement, their order of influence will be considered and discussed.

We do not want to focus on the application, functionality and usability of the powder and coating pairings, but only try to evaluate the thickness of the coatings. Thickness determination methods other than resistance measurement are presented only briefly as complementary methods and are used to validate and explain the results obtained here. Further information on these methods can be found in the quoted references.

2. Materials and methods

In this section the setup for measuring the electrical resistance under increasing, external load is presented. To obtain a basic understanding of the investigated powders and their possible behaviour during deposition and resistance measurement, a basic analysis of the granules is performed and summarized. Additionally the coating system for powders and complementary gravimetric and optical methods for thickness determination are discussed. Finally the used coating materials, coating parameters and storage conditions are presented.

2.1. Electrical resistance measurement

The electrical resistance measurements under increasing, external load were performed in a custom designed measurement setup, which is outlined in Fig. 1. The basic components are a fixed lower copper electrode with a thick insulating, transparent PMMA cylinder holding the granulate sample and a close-fitting copper piston acting as an upper electrode. This is a common concept reported in other works [29–32]. However, the upper electrode was specifically designed in a way that the contact area with the cylinder does not increase during further insertion but remains constant from a certain point onwards, see “fixed friction area” in Fig. 1b. In this system both electrodes are mounted onto an insulating intermediate cylinder made of PTFE, which in turn is mounted to a tensile and compressive load cell (ME Messsysteme KM26z: 2 kN), with the lower cell attached to the frame and the upper cell attached to a guided, motorized spindle drive. In order to avoid deformation by the forces applied, the frame was composed of rigid profiles (Bosch Rexroth 40 x 40 mm) and angles, reinforced with two 2 cm thick aluminium plates. The resistance between the two copper electrodes is measured using an Agilent 34410A two-point resistance meter. The applied force, the resistance as well as the position of the piston are recorded. It should be noted that due to this special design not only compaction processes can be measured, but also a measurement during the decompression of the powder is possible.

To ensure reliable resistance measurements certain measures and routines must be adhered to. Before each measurement a zeroing of all electrical measuring devices is performed. The first step is to zero both load cells and calibrate the height. To do this, the electrodes are brought together. When contact is made and a minimum force threshold (greater than 2 N) is reached, the height is set to zero. During this procedure the system resistance is recorded and this value is an indicator for the surface condition of the electrodes. Regardless of this value, the contact surfaces of the two electrodes were regularly polished.

For light powders in combination with large measurement volumes, a pre-compaction routine was applied to obtain reliable measurements. The desired amount of powder was filled into the sample cylinder connected to the lower electrode. This filled assembly was shaken on a sieve shaker (Retch AS200) for defined times and amplitudes. Specifically, 30 s with an amplitude setting of 50 followed by 30 s with an amplitude setting of 70. This was applied to HGM samples only, as no significant improvement was observed for NMC811.

2.2. Powders

The powders used are hollow glass microspheres [33] (HGMs) with an anti-caking agent applied to their surface and NMC811 (stabi-

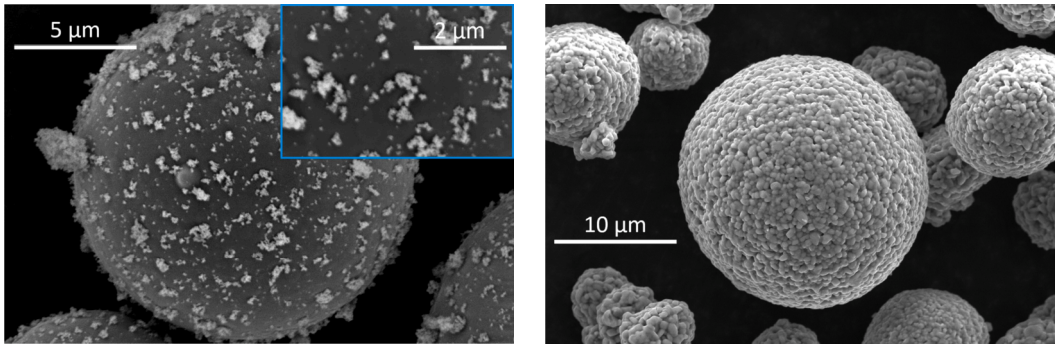

(a) HGMs with anti-caking agent (b) Stabilized NMC811

Fig. 2. SEM images of single particles of (a) HGMs with anti-caking agent (white hunks on the spheres) and (b) stabilized NMC811.

Table 1
Mean grain diameter d_p determined on the number of found grains N_i on microscope images compared to D50 diameters d_m specified by the manufacturer. In addition, the tap density ρ_m determined by the supplier is given.

powder	sieve size	d_m	ρ_m	d_p	N_i
	µm	µm	g cm^{-3}	µm	
S38	≥ 71			78 ± 5	397
S38	71 - 63			66 ± 4	596
S38	63 - 50			55 ± 4	797
S38	50 - 40			45 ± 4	2080
S38	-	40	0.38	19 ± 12	1438
stabilized NMC811	-	11.2	2.3	8 ± 2	240
non-stab. NMC811	-	10.38	2.53	7 ± 3	6431

lized [34] and non-stabilized [35]) powders. In this case, stabilization means that the grains of the NMC811 are protected from oxidation by the manufacturer using an unknown process.

As a first step an inspection under an optical microscope is performed. Two main factors, the sphericity Ψ and the mean diameter d_p, are determined. Image analysis is performed with a Reichert-Jung Polyvar MET optical microscope and the program ImageJ [36], although only the roundness, which is the two-dimensional equivalent of the sphericity, of the powder can be determined here. The procedure used is applying a threshold to the image and finding and analysing the particles within the desired criteria for roundness and size. Fig. 2 shows scanning electron microscope (SEM) images of the powders. It can be seen, that the HGMS (Fig. 2a) are almost perfectly round which is why the sphericity is $\Psi = 1$. In the case of NMC811 (Fig. 2b), a sphericity of $\Psi = 0.9$ was found, within the resolution limit of the optical images used.

The size distribution of particles in powders can be described mathematically by a distribution [37] such as the log-normal distribution. Here, the mean size of powders is simply calculated by taking the arithmetic mean of all detected particles on several images for each size class. Table 1 shows the found mean diameters of all used powders. The HGMs where sieved with a sieve shaker (Retch AS200) at various wire mesh sizes, to examine the effect of different size classes of coated powders on the resistance measurements.

2.3. Powder coating system

The powders were coated by magnetron sputtering in a specially designed coating system [38] built and described in detail by Eder et al. [3]. Fig. 3 shows a 3D-model of the sputter system used. The key feature of the system is the movable container which can hold up to 1000 cm^3 of powder. The tilted and rotating circular plate on top of which the container is freely positioned ensures efficient intermixing and a uniform coating. This intermixing is necessary due to the line-of-sight nature of the sputtering process. In addition to rotation, the circular plate is equipped with a variable number of concussion

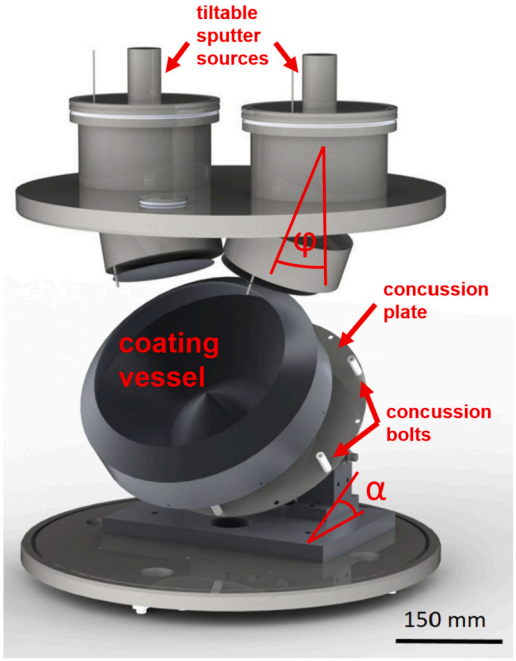

Fig. 3. 3D-model of the magnetron sputtering system for powder coatings.

bolts, which lift the container until the centre of gravity is no longer supported. Without any support, the coating container slides down the tilted circular plate, also called concussion plate, until it is stopped by another pair of pins. The occurring concussion, supported by the rotation of the coating vessel, prevents possible agglomeration of the powder under vacuum conditions. The strength of the impact can be regulated by adjusting the tilt angle α of the concussion plate. To ensure maximum exposition of the powder to the vapour beam, the two magnetron sputter sources can be individually tilted by the angle φ and rotated on the vacuum flange.

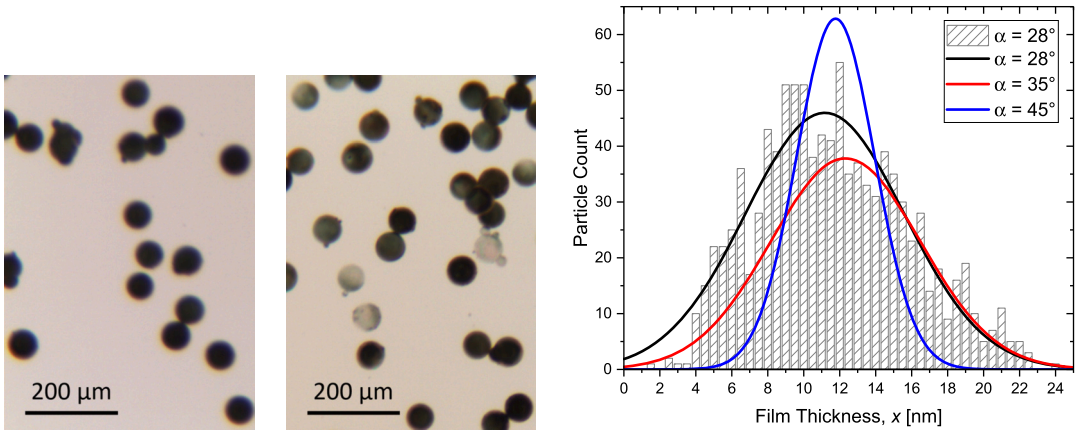

(a) Homogeneous $\alpha = 35°$ (b) Inhomogeneous $\alpha = 28°$ (c) Particle statistics

Fig. 4. Optical analysis of copper-coated HGMs. (a) Homogeneously coated HGMs under $\alpha = 35°$, (b) inomogeneously coated HGMs under $\alpha = 28°$ and (c) best gaussian fit of average layer thickness distribution of detected particles at different steepnesses α of the concussion plate.

There are some known methods for determining the film thickness on granules, which are usually time-consuming and involve only a few particles. Depending on the particle size, there are up to 10^{10} particles per 1000 cm^3 of powder (see Table 1) and thus measuring the film thickness on single particles is not feasible.

Assuming uniform coating of all particles in the batch, the calculation of the average coating thickness x [3] is possible by inserting the sputter rate determined on a flat substrate R at the height of the surface of the powder bed in the coating container, the exposed powder area in the container A_{expo}, the powder volume $V_{substrate}$, the sphericity Ψ, the packing factor f and the coating time t into Equation (1):

$$x = \frac{r_p R t A_{expo} \Psi}{3 V_{substrate} f} \tag{1}$$

2.3.1. Gravimetry

A very simple and effective way to determine the average film thickness x of a batch of coated powder [3] is to measure the increase of mass m_{film} after coating according to

$$x = r_p \left(\sqrt[3]{\left(\frac{m_{film} \Psi}{\rho_{film} f V_{substrate}} \right)} + 1 - 1 \right). \tag{2}$$

Equation (2) describes the average film thickness on a particle depending on the total mass increase due to the coating $m_{film} = V_{film} \rho_{film}$ equally distributed to all particles N with a mean radius r_p. The amount of particles N contained in the coated volume $V_{substrate}$ of powder can be calculated using the mean particle radius r_p and including the packing factor $f = 0.60 \pm 0.05$. The sphericity Ψ of the particles must also be taken into account and is discussed in subsection 2.2 for the examined powders. Here, the gravimetric measurements are used as a main reference for comparison with the resistance measurements.

2.3.2. Optical transmission

In case of a transparent substrate and transparent absorbing layer [27], it is also possible to measure the reduction in transmission described by the Beer-Lambert law

$$T = \frac{I}{I_0} = e^{-\alpha d}. \tag{3}$$

In Equation (3) I_0 is the intensity of an incident light beam, I is the intensity after passing the particle including two times the layer, α is the extinction coefficient of the absorbing material and d is the thickness of the material. A simple way to measure intensities is to evaluate the RGB channels of an image taken from a CCD chip in a microscope or an image from a high-resolution scanner. Therefore, a single layer of granulate needs to be prepared and agglomerations should be avoided. To obtain proper statistics of individual grains with a defined size, an object identification algorithm can be applied to the image. When considering the entire grain, an error is made at the edges of the grains where the film is tilted or perpendicular to the image plane. Thus, knowing the size of the grain and using simple geometry, the imaged grains can be reduced to their core where roughly plane-parallel surfaces exist.

Fig. 4 shows the achievable film thickness homogeneity of copper-coated HGMs under different tilts α of the concussion plate determined by the optical method. As can be clearly seen in Fig. 4c, a narrower distribution of average thicknesses on the particles is observed as α increases, but a comparable mean thickness of the powder batch is maintained. The relative error of the thickness can be estimated from this plot to be about 30 %. For this statistical analysis and the application of the above described evaluation steps, the ThinFilmInspect program package created by Mahr [39] was used.

2.4. Coating materials

The sputtering materials were commercially available technical copper (E-Cu 2.0060, Norm: DIN 1751), purity 99.9 %, aluminium (Al99.5, Norm: AW-1050A), purity 99.5 %, silver, purity 99.99 % and zirconium, Zr grade 702, supplied by Kurt J. Lesker. The two simultaneously used targets are 4 inch diameter discs with a height of 5 mm to 6 mm.

2.5. Coating parameters and powder storage

The coating and storage conditions of the powders are of vital importance for the findings of this work. Table 2 shows a full overview of the used coating parameters.

For coating the HGMs, two containers were used, a large container with a maximum filling volume of 1000 cm^3 (called SuperBowl, SB) and a medium container with a filling volume of 100 cm^3 (called MediumBowl, MB). For all copper coatings, the large container was used and 1000 cm^3 of HGMs were coated. For silver and aluminium, on the other hand, the MB and only a quantity of 100 cm^3 powder was used to reduce the coating time and material cost. The prediction of the coating thickness x_{pred} was calculated from rate measurements on flat substrates (see Equation (1)) and using the mean diameters in Table 1. When comparing the predicted coating thickness to gravimetric measurements according to Equation (2) a good agreement could be found.

The NMC811 powder was coated in the SB with Al_2O_3 and ZrO_2 by reactive DC magnetron sputtering. The oxygen flow was adjusted so that the operating point of the discharge was at the beginning of the

Table 2
Coating Parameters: P power per coating source, α tilt angle of concussion plate, t coating time in h or min, x_{pred} predicted coating thickness from coating rate on flat substrates, x_{gravi} thickness calculation from increase in mass on the powder.

Vessel	$V_{substrate}$	Substrate	Material	P	α	t		x_{pred}	x_{gravi}	Comment
	dm^3			W	°	h	min	nm	nm	
			Thickness							
SB	1	HGM	Cu	2x1000	35	1.5		5.4	4.5	
SB	1	HGM	Cu	2x1000	35	3.5		12.5	12.2	
SB	1	HGM	Cu	2x1000	35	5.5		19.6	17.7	
SB	1	HGM	Cu	2x1000	35	7.5		26.7	27.9	
SB	1	HGM	Cu	2x1000	35	9.5		33.9	30.9	
MB	0.1	HGM	Al	1x900	35	3.0		9.3	11.7	optimized for one source
MB	0.1	HGM	Al	1x900	35	7.0		21.8	25.3	optimized for one source
MB	0.1	HGM	Al	1x900	35	9.0		28.0	36.0	optimized for one source
MB	0.1	HGM	Ag - inhomo.	1x1000	35		20	6.7	6.3	
MB	0.1	HGM	Ag - inhomo.	1x1000	35		45	15.2	15.1	
MB	0.1	HGM	Ag - inhomo.	1x1000	35		60	20.2	21.4	
MB	0.1	HGM	Ag - inhomo.	1x1000	35		80	27.0	27.4	
MB	0.1	HGM	Ag - inhomo.	1x1000	35		100	33.6	37.6	
MB	0.1	HGM	Ag - homo.	1x500	45		80	11.0	10.1	optimized for one source
MB	0.1	HGM	Ag - homo.	1x500	45		160	22.1	-	optimized for one source, loss of powder during coating
MB	0.1	HGM	Ag - homo.	1x500	45		240	33.1	-	optimized for one source, loss of powder during coating
			Tilt and Distribution							
SB	1	HGM	Cu	2x1000	28	3.5		12.3	11.2	
SB	1	HGM	Cu	2x1000	45	3.5		7.5	8.2	
SB	0.1	stabilized NMC811	Al_2O_3	2x900	45		5	0.19	-	Ar: 17 sccm (0.4 Pa), O_2: 15 sccm
SB	0.1	stabilized NMC811	Al_2O_3	2x900	45		10	0.38	-	Ar: 17 sccm (0.4 Pa), O_2: 15 sccm
SB	0.1	stabilized NMC811	Al_2O_3	2x900	45		20	0.77	-	Ar: 17 sccm (0.4 Pa), O_2: 15 sccm
SB	0.1	stabilized NMC811	Al_2O_3	2x900	45		40	1.75	-	Ar: 17 sccm (0.4 Pa), O_2: 15 sccm
SB	0.1	stabilized NMC811	ZrO_2	2x600	45		5	0.20	-	Ar: 17 sccm (0.4 Pa), O_2: 12.5 sccm
SB	0.1	stabilized NMC811	ZrO_2	2x600	45		10	0.4	-	Ar: 17 sccm (0.4 Pa), O_2: 12.5 sccm
SB	0.1	stabilized NMC811	ZrO_2	2x600	45		20	0.8	-	Ar: 17 sccm (0.4 Pa), O_2: 12.5 sccm
SB	0.1	stabilized NMC811	ZrO_2	2x600	45		40	1.6	-	Ar: 17 sccm (0.4 Pa), O_2: 12.5 sccm
SB	0.1	non-stab. NMC811	ZrO_2	2x600	45		33	1.0	-	Ar: 17 sccm (0.4 Pa), O_2: 12.5 sccm
SB	0.1	non-stab. NMC811	ZrO_2	2x600	45		66	2.0	-	Ar: 17 sccm (0.4 Pa), O_2: 12.5 sccm
SB	0.1	non-stab. NMC811	ZrO_2	2x600	45		100	3.0	-	Ar: 17 sccm (0.4 Pa), O_2: 12.5 sccm
SB	0.1	non-stab. NMC811	ZrO_2	2x600	45		133	4.0	-	Ar: 17 sccm (0.4 Pa), O_2: 12.5 sccm
SB	0.1	non-stab. NMC811	ZrO_2	2x600	45		166	5.0	-	Ar: 17 sccm (0.4 Pa), O_2: 12.5 sccm
SB	0.1	non-stab. NMC811	ZrO_2	2x600	45		199	6.0	-	Ar: 17 sccm (0.4 Pa), O_2: 12.5 sccm

hysteresis region of the reactive sputtering process (see, e.g. [40]) to achieve maximum deposition rates without poisoning the target or observing arcing. A lower powder volume of $100\,cm^3$ was used compared to the copper coated HGMs. The reason for this reduction in filling volume is the lower sputtering yield of oxides compared to the non-reactive sputtering mode of the same materials [40].

Compared to the HGMs, where weight measurements were used to calculate the layer thickness, only the prediction method (see Equation (1)) was used for NMC811. With coated HGMs it was found that the prediction model is in very good agreement with the thickness calculation from gravimetric measurements. The reason gravimetry was omitted for the NMC811 powder is the ratio between weight of the coating to the weight of the powder, which can be seen when comparing the densities given in Table 1, and the fact that chipping of coating material on the container into the powder cannot be neglected. For example, the total mass increase when coating $100\,cm^3$ of NMC811 powder, weight $253\,g$, with a $2\,nm$ Al_2O_3 coating is about $1\,g$ and amounts to $0.4\,\%$ of the total mass. With HGMs on the other hand, even in the worst case the ratio of coating mass to powder mass amounts to $5.7\,\%$.

The size distribution of the delivered powder is often subject to large variances, HGM particle diameters are shown in [3] and NMC811 is shown in [41]. Unfortunately, this wide distribution leads to large relative errors when calculations are performed with the determined average diameter. For this reason the error for the calculated thicknesses in this article is omitted.

Within one powder/coating pairing the only variable parameter is coating time. The predicted coating thickness was calculated from the coating time in order to obtain a consistent representation of the different coatings.

In general oxidation or degradation of the powder or of the coating on the powder influences the electrical resistance. This is why storage conditions are discussed here. Because of the large volume of powder, uncoated as well as coated, HGMs were stored under atmospheric conditions. Uncoated HGMs are delivered in batches of $50\,dm^3$ in sealed bags. Up to $1000\,cm^3$ of coated HGMs was stored in plastic storage containers. NMC811 was delivered in sealed containers filled with inert gas in batches of $1000\,cm^3$. After breaking the seal as well as after coating the NMC811 powder containers were stored in low vacuum conditions in a dessicator.

3. Results and discussion

The dependence of the resistance measurement under increasing load on the film thickness and other possible influence factors like coating inhomogeneity of different coating material and powder combinations is discussed. Selected measurements are then considered within the concept of force per grain to reduce measurement parameter dependency.

Fig. 5 shows resistance curves for the powders presented in subsection 2.2. Electrodes with a diameter of 2 cm have been used in this and all other experiments presented in this work. Uncoated HGMs are insulators and show no significant dependence of the resistance on the applied force, only after coating with a sufficiently thick layer of conductive material a typical resistance curve (see Fig. 6) is found. Since NMC811 is classified as a semi conductor, a baseline measurement of uncoated powder is of interest. It can be seen that the electrical resistance of the powder, as received, is already dependent on the applied force. A significant difference between uncoated non-stabilized and stabilized NMC811 can be found. The percolation force (see Fig. 5 and related text) is significantly higher for stabilized than for the non-stabilized NMC811 powder.

In Fig. 6 typical resistance curves under increasing, external load of a non-conductive powder (HGMs) coated with conductive material (Cu) of different thicknesses is displayed. Four different stages

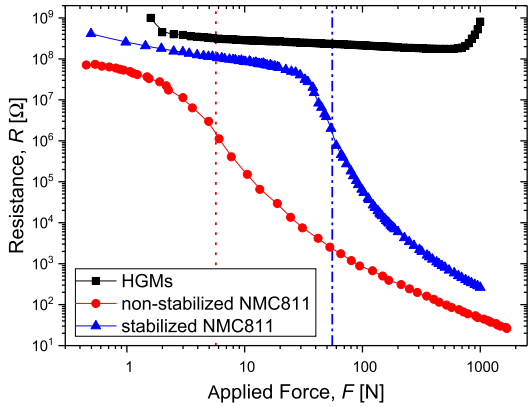

Fig. 5. Typical resistance curves for each used powder with marked percolation force (broken vertical lines).

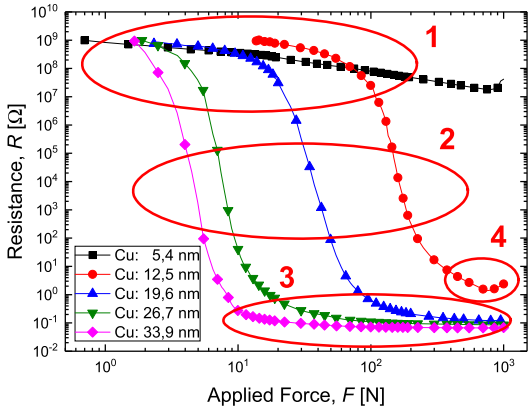

Fig. 6. Distinctive resistance curve under increasing, external load of non-conductive HGMs coated with different thicknesses (predicted) of copper. (1) Powder compaction, (2) reaching percolation threshold, (3) saturation after threshold and (4) plastic deformation.

can be identified, which is in good agreement with the Heckel profile [42,43] describing the process of powder compaction. In the first stage (1) the powder is compacted and contacts of the surface oxide are formed. After forming enough contacts and applying more pressure a threshold (2) is reached. The initially high contact resistance, due to the surface oxide, decreases because of the increasing contact area with the underlying conductive material. The observed phenomenon is well known and can be described by the theory of percolation [44,45]. Percolation theory describes the formation of connected areas in disordered systems by a so-called percolation threshold. Upon reaching the threshold (3), the powder column becomes conductive and a saturation resistance is reached. No further reduction of the resistance is reached when increasing the applied force. After particle rearrangement and elastic deformation comes the regime of plastic deformation (4). Plastic deformation in the case of coated, fragile hollow particles means fragmentation of individual spheres and thereby an increase in resistance. Here, stage (4) is only observed at lower layer thickness (data set: red circles) where percolation was not fully completed.

From Fig. 6 it can be concluded, that the appearance of this characteristic curve indicates the presence of a conductive coating with a certain thickness on non-conductive powder. Furthermore a clear dependence of the position of the inflection point (2) on the different predicted film thicknesses, resulting from changing the coating time only, can be seen. The force required to reach the inflection point, which can be associated to the percolation threshold, will be referred to as the percolation force F_{percol} and can be considered as a measure for the coating thickness. However, other influencing factors cannot

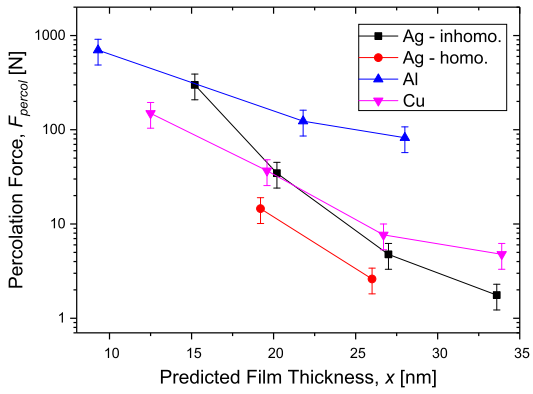

Fig. 7. Comparison of percolation force F_{percol} of silver, aluminium and copper coatings on HGMs depending on the predicted film thickness x. The detectability of the inhomogeneity of the coating is demonstrated on silver coated HGMs.

yet be excluded from this observation. The statistical nature of powder compaction makes it very difficult to calculate an absolute value of the percolation threshold in advance. The thickness given in all displayed graphs was calculated by the prediction method described in subsection 2.3. In this work, all measurements are considered relative and comparative.

Additionally, oxidation of the powder or the coating is a possible influence to the displayed electrical resistivity curves. Usually electrical resistivity measurements were carried out within days after coating a batch, except when sieving the coated batch into different size classes. This takes two to three additional days to reach the amount required for the measurements. Long-term stability of copper coated HGMs was tested by repeated measurements of samples of one coating batch over months. A statistically significant change could only be observed after three months.

The shape of the curves given in Fig. 6 was explained using the Heckel profile and the percolation theory. In addition, the force at the inflection point, the so called percolation force F_{percol}, was identified as a characteristic value associated to the film thickness. The inflection point of the measurement data is calculated numerically by resampling the data to equidistant data points, smoothing the data with a Savitzky–Golay filter, deriving the resulting data using second order accurate central differences, smoothing the derivation with a Savitzky–Golay filter, and finding the minimum of the derivative that corresponds to the inflection point.

To determine the reproducibility of resistance measurement and subsequent determination of the percolation force, two experimental series, one with copper-coated HGMs and one with ZrO_2-coated NMC811 powder, were performed. For copper-coated HGMs, a relative statistical error of 30.47 % of the percolation force was determined after 38 measurements under identical conditions. To validate the found relative error of HGMs for a different powder, a second series was performed with equal results. On ZrO_2-coated NMC811 powder a relative statistical error of 27.66 % was determined after 24 measurements. With these results the relative accuracy of the resistance measurement setup and subsequent determination of the percolation force can be put at about 30 %, independent of the powder.

Fig. 7 shows the determined percolation force of 5 cm^3 of HGMs coated with different materials of different predicted thicknesses. The error bars in Fig. 7 result from the relative error in F_{percol} discussed above. A clear distinction between different predicted coating thicknesses can be made. Comparing the differences in coating materials, it can be argued that aluminium has the highest resistivity and the least elastic [46,47] oxide layer and therefore requires the highest percolation force. When comparing silver and copper, the latter has a slightly higher resistivity and both have a lower resistivity than aluminium. Fig. 7, however, shows that silver coatings at a first glance have a higher

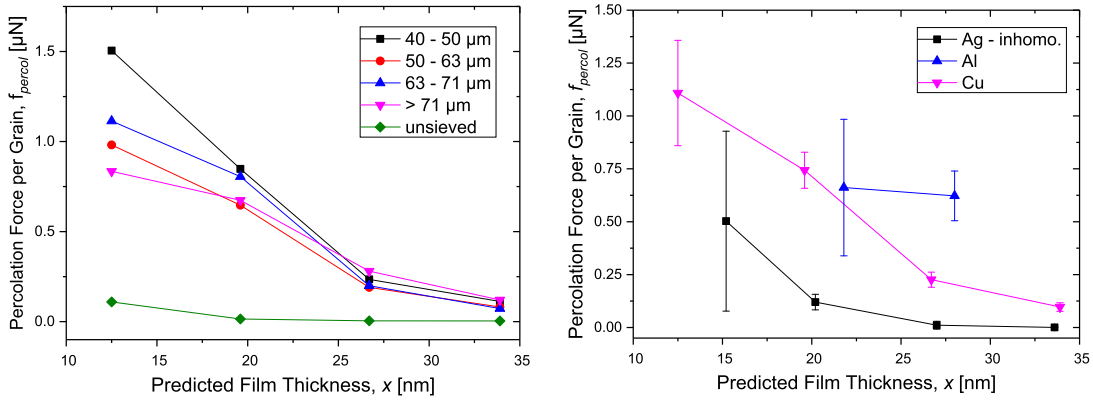

(a) Copper (b) Materials

Fig. 8. Dependence of percolation force per grain f_{percol} on predicted coating thickness x of (a) copper coatings on HGMs separated into different size classes and (b) silver, aluminium and copper coatings on HGMs. The error bars result from the average of the measured percolation force of the coated HGMs over all size classes (listed in Table 1) excluding the unsieved coated HGMs.

percolation force at lower thicknesses than copper coatings (Fig. 7, data set: black squares). This phenomenon can be attributed to inhomogeneous coatings of silver which was confirmed by optical transmission measurements. When fine tuning the coating parameters, a more homogeneous silver coating can be deposited and a significantly lower percolation force is found (Fig. 7, data set: red circles).

In general, the percolation force decreases with increasing film thickness to a point where the sensitivity of the measuring device is too low to capture the characteristic resistance curve, and only the saturation resistance (see Fig. 6, (3)) is measured. If lower film thicknesses are considered, no percolation force can be determined and only the base resistance is measured. In case of the HGMs, the fracture of the HGMs limits the maximum achievable percolation force, which was found to be more than 700 N with a 2 cm diameter electrode.

It is therefore clear that the measurement window in which the percolation curve of a powder can be fully accessed is limited. Therefore, the influence of different measurement parameters on the percolation force was investigated during the characterization of the measurement setup. Varied and tested parameters (not displayed) were: electrode diameter, filling level, filling volume, particle size, number of particles and electrode (compaction) speed. Despite all calibration measurements, the quantification of the absolute film thickness was not possible and, in the best case, would only be possible by the production of well-defined calibration samples.

After these measurements, it became apparent that the percolation force of one powder, material and thickness combination is equal when the same number of particles is measured. Therefore, the concept of percolation force per grain f_{percol} was introduced, where $f_{percol} = F_{percol}/N$ with N as the number of particles in the powder sample under consideration.

To perform measurements based on the above concept, the coated batch of HGMs was separated into different size classes determined by the mesh size of the sieve used (listed in Table 1). For consistency, all these measurements were performed with identical measurement parameters. 5 cm^3 of sieved powder was measured with the 2 cm diameter electrode. Fig. 8a shows the change of percolation force per grain f_{percol} over coating thickness for copper coated HGMs separated into different size classes. It is visible that the variance of the percolation force per grain decreases with increasing film thickness. Furthermore, it can be seen that small diameter particles have the highest and large diameter powders the lowest percolation force per grain. One possible explanation is the inhomogeneity of thin coatings on small sized grains because of low coating times and thus low intermixing. This was confirmed by the optical analysis method, described in subsubsection 2.3.2, where coated HGMs with a smaller diameter show lower film thicknesses when compared to HGMs of larger diameter within the coated batch.

Fig. 8b shows the percolation force per grain f_{percol} for HGMs coated with different materials of different thicknesses. The error bars result from the average of the measured percolation force of the coated HGMs over all size classes (listed in Table 1) without the unsieved coated HGMs. Unsieved HGMs were not considered because of the wide distribution of particle diameters [3] when compared to the sieved particles. The effect of this wide size distribution on the percolation force per grain can be seen in Fig. 8a for the example of copper. A similar decrease in the spread of the percolation force per gain with increasing film thickness can be observed for all materials.

For HGMs it can be concluded that it is possible to qualitatively determine differences in the thickness of a coating material. Whether the observed shift in percolation force is due to thickness or to inhomogeneity at lower thicknesses is not known. When comparing the same material at the same average thickness it is possible to compare the homogeneity of the coating. Furthermore, the concept of percolation force per grain f_{percol} was introduced to reduce the dependence of the resistance measurement on measurement parameters, since filling volume and mean particle diameter directly influence the number of investigated particles. The difference in coating thickness for different classes of particle diameter within the same coating batch can also be deduced by looking at the force per grain. The assertion of a size dependent thickness was verified using the optical measurement method discussed in subsubsection 2.3.2.

All the above considerations were made using the HGMs as a non-conductive base powder. To test whether the phenomena found and described could be transferred to another class of powders, NMC811 was selected as a second, conductive, candidate. In this case, we coated the conductive powder with a non-conductive oxide and analysed the resistance behaviour.

Similar to HGMs a long-term stability test of the percolation force of non-stabilized NMC811 powder was carried out. It was found, that storage of non-stabilized NMC811 under atmospheric conditions significantly changes the percolation force only after four weeks. Therefore, all NMC811 samples were stored under low vacuum conditions.

Fig. 9 shows the percolation force per grain f_{percol} of non-stabilized and stabilized NMC811 coated with Al_2O_3 and ZrO_2. The measurement volume of stabilized NMC811 was 0.625 cm^3 and 0.5 cm^3 for non-stabilized NMC811, which proved to be the optimal amount for the deposited thicknesses. When comparing Al_2O_3 with ZrO_2 on stabilized NMC811, no difference in f_{percol} is observed. In contrast, when comparing non-stabilized with stabilized NMC811, a clear offset of f_{percol} can be observed for stabilized NMC811. The most reasonable assertion is that the unknown stabilisation process used by the manufacturer involves the application of a non-conductive layer in the thickness range of 1 nm to 2 nm on the powder.

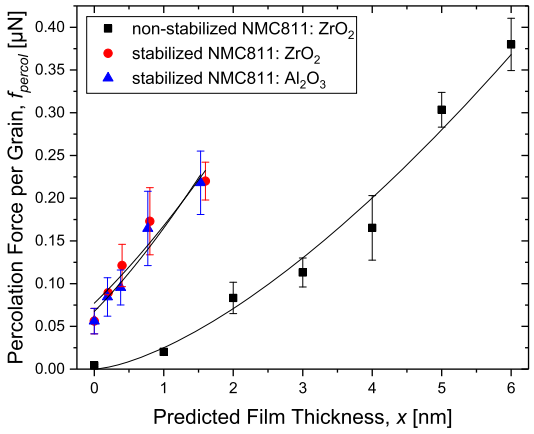

Fig. 9. Average percolation force f_{percol} per grain of different oxide coatings on non-stabilized and stabilized NMC811 over the predicted thickness of the film x. Average results from at least three measurements.

The thickness of this unknown passive layer can be calculated by fitting the data within the framework of Hertz' contact theory as described by Kurinjimala et al. [41]. It is assumed that the insulating coating fails at the percolation force per grain. Then the deformation, described within the framework of the Hertzian contact theory, can be assumed to be equal to the coating thickness x and an eventual additional layer with the thickness x_0. Following this approach, the layer thickness x_0 can be evaluated by fitting the percolation force per grain according to

$$f_{percol} = A\left(x + x_0\right)^{\frac{3}{2}} \tag{4}$$

where the fitting parameter A reflects the effective mechanical properties of the coated spherical particles. The fits for all data give x_0 = 0.00 nm ± 0.21 nm for non-stabilized NMC811, x_0 = 1.23 nm ± 0.39 nm for Al_2O_3 coated stabilized NMC811 and x_0 = 1.47 nm ± 0.26 nm for ZrO_2 coated stabilized NMC811, which is in good agreement with the initial assumption. The fitting parameter A was omitted because no further information could be extracted.

Here, it is not possible to estimate the uniformity of the coating with this measurement method nor with an optical transmission method. However, low voltage energy selective backscatter (ESB) SEM images of stabilized NMC811 coated with Al_2O_3 and ZrO_2 where taken [41], and in both cases a uniformly distributed oxide layer was observed when compared to uncoated NMC811.

In conclusion, the percolation force of NMC811 coated with a non-conductive film was expected to increase with the thickness of the coating. To validate this, oxide layers of different thicknesses were deposited onto conductive NMC811 powder. In doing so, the resistance curve could be manipulated as expected. Increasing the oxide layer thickness on the conductive powder results in higher forces required to form fully connected paths through the powder sample. Furthermore, the performance of this measurement method became apparent when comparing non-stabilized and stabilized NMC811, where the presence of an additional layer which could not be observed by SEM could be immediately inferred.

The behaviour of NMC811 coated with a non-conductive film can be described within the framework of Hertz' contact theory. The behaviour of HGMs a non-conductive substrate coated with conductive material cannot be explained by this theory. An intuitive explanation for this phenomenon is that this measurement is strongly influenced by the inhomogeneity of the layer thickness on different grains. In terms of percolation theory only particles with sufficient conductive material can be percolation sites. If one assumes inhomogeneous coating and compares batches of the same powder/coating combinations at different coating times, then longer coating times result in more percolation sites for the same quantity of powder considered. It must be pointed out that these statements cannot be answered completely with the measurements presented here.

In order to confirm or disprove the established hypotheses, further experiments must be carried out. First, monodisperse HGMs should be coated and the homogeneity of the film should be thoroughly analyzed. Assuming that monodisperse HGMs are absolutely uniformly coated, only the effect of coating thickness on the electrical resistance can be studied. For investigation in terms of percolation theory, a mixture of coated and uncoated monodisperse HGMs in a certain mixing ratio can be investigated. Thus, the influence of the inhomogeneity in layer thickness on different particles can be approximated.

4. Conclusions and outlook

It has been shown that both heavy and light powdery substances with small diameters up to a volume of 1000 cm^3 can be homogeneously coated with conductive and non-conductive materials with thicknesses in the nm range. Several methods for determining absolute coating thickness were briefly discussed. The resistance measurement under increasing, external load has been proven to be a very powerful, versatile and quick complementary method for detecting and studying film thickness, overall film homogeneity, and film homogeneity on different particle size classes.

In both presented application cases it was possible to detect very thin coatings with the discussed method. For NMC811 coating time differences resulting in predicted average layer thickness differences of as low as 1 nm can be resolved. In case of HGMs coating time differences resulting in predicted average layer thickness differences of 5 nm to 10 nm can be resolved, above a material-dependent minimal thickness.

The initial load dependent resistivity of uncoated NMC811 verifies the presented stages of the powder compaction. The expectation that the percolation process is further hindered by the application of an insulating layer, even an inhomogeneous one, is therefore reasonable.

This explanation is not applicable to HGMs where the applied film thickness increases and the associated percolation force decreases. However, a clear dependency of the percolation force on the coating thickness was found. In the present experiments, it is not clear whether the dependence found is due to increase of average thickness or is caused by the increasing homogeneity of the coating with increasing thickness.

To fully exploit the potential of the presented method, a well-posed problem must be addressed. For example, in a production environment, it would be necessary to establish an empirical relationship between thickness and percolation force from well-prepared calibration samples. When knowing the thickness, the homogeneity can be tested. In contrast, when not knowing the thickness, the combined effect of coating thickness and homogeneity is evaluated.

The discussed analysis method has high sensitivity for powder and coating combinations with a high conductivity contrast and is particularly useful when dealing with ultra thin coatings or heavy powders, where gravimetric measurements become inaccurate due to the small relative mass increase resulting from the coating.

CRediT authorship contribution statement

David Böhm: Writing - Original Draft, Investigation, Methodology, Writing - Review & Editing, Data Curation. **Matija Kusztrich:** Investigation, Review. **Robin Kurinjimala:** Investigation, Review. **Eder Andreas:** Supervision, Methodology, Conceptualization, Review. **Christoph Eisenmenger-Sittner:** Funding acquisition, Project administration, Supervision, Review.

Declaration of competing interest

The authors declare that they have no known competing financial interests or personal relationships that could have appeared to influence the work reported in this paper.

Data availability

Data will be made available on request.

Acknowledgements

This work is supported by the Austrian "Fonds zur Förderung der Wissenschaftlichen Forschung" (FWF) under Grant Nr.: TRP-281-N20. The SEM studies were performed with the facilities of the University Service Center for Transmission Electron Microscope (USTEM), TU Wien, Austria.

References

[1] J. Li, G.-K. Ren, J. Chen, X. Chen, W. Wu, Y. Liu, X. Chen, J. Song, Y.-H. Lin, Y. Shi, Facilitating complex thin film deposition by using magnetron sputtering: a review, JOM 74 (2022) 3069–3081, https://doi.org/10.1007/s11837-022-05294-0.

[2] G. Schmid, C. Eisenmenger-Sittner, A method for uniformly coating powdery substrates by magnetron sputtering, Surf. Coat. Technol. 236 (2013) 353–360, https://doi.org/10.1016/j.surfcoat.2013.10.012.

[3] A. Eder, G.H.S. Schmid, H. Mahr, C. Eisenmenger-Sittner, Aspects of thin film deposition on granulates by physical vapor deposition, Eur. Phys. J. D 70 (2016) 247, https://doi.org/10.1140/epjd/e2016-70435-7.

[4] J.L. Priedeman, G.B. Thompson, Conformal coating of powders by magnetron sputtering, Surf. Coat. Technol. 436 (2022) 128242, https://doi.org/10.1016/j.surfcoat.2022.128242.

[5] Y. Zhang, Z. Su, J. Shang, Uniform sputtered metallic coatings on silica glass micro shell resonators, in: 2022 23rd International Conference on Electronic Packaging Technology (ICEPT), IEEE, 2022, pp. 1–4.

[6] H.V. Atkinson, S. Davies, Fundamental aspects of hot isostatic pressing: an overview, Metall. Mater. Trans. A 31 (2000) 2981–3000, https://doi.org/10.1007/s11661-000-0078-2.

[7] J. Lu, L. Gao, J. Sun, L. Gui, J. Guo, Effect of nickel content on the sintering behavior, mechanical and dielectric properties of Al2O3/Ni composites from coated powders, Mater. Sci. Eng. A 293 (2000) 223–228, https://doi.org/10.1016/s0921-5093(00)01231-4.

[8] M. Li, H.-L. Huang, J.-M. Wu, Y.-R. Wu, Z.-A. Shi, J.-X. Zhang, Y.-S. Shi, Preparation and properties of Si3N4 ceramics via digital light processing using Si3N4 powder coated with Al2O3-Y2O3 sintering additives, Addit. Manuf. 53 (2022) 102713, https://doi.org/10.1016/j.addma.2022.102713.

[9] R. Unnikrishnan, J. Gardy, B.F. Spencer, R. Kurinjimala, A. Dey, V. Nekouie, S. Irukuvarghula, A. Hassanpour, C. Eisenmenger-Sittner, J.A. Francis, M. Preuss, Functionalization of metallic powder for performance enhancement, Mater. Des. 221 (2022) 110900, https://doi.org/10.1016/j.matdes.2022.110900.

[10] Y. He, A. Hassanpour, A.E. Bayly, Combined effect of particle size and surface cohesiveness on powder spreadability for additive manufacturing, Powder Technol. 392 (2021) 191–203, https://doi.org/10.1016/j.powtec.2021.06.046.

[11] S. Matsusaka, H. Maruyama, T. Matsuyama, M. Ghadiri, Triboelectric charging of powders: a review, Chem. Eng. Sci. 65 (2010) 5781–5807, https://doi.org/10.1016/j.ces.2010.07.005.

[12] G.C. Righini, Glassy microspheres for energy applications, Micromachines 9 (2018) 379, https://doi.org/10.3390/mi9080379.

[13] H. Zhang, F. Wang, J. Liang, Q. Tang, Y. Chen, Design of thermal insulation energy-saving coatings for exterior wall, Chem. Eng. Trans. 61 (2017) 1207–1212, https://doi.org/10.3303/CET1761199.

[14] A. Synnefa, M. Santamouris, H. Akbari, Estimating the effect of using cool coatings on energy loads and thermal comfort in residential buildings in various climatic conditions, Energy Build. 39 (2007) 1167–1174, https://doi.org/10.1016/j.enbuild.2007.01.004.

[15] C.B. Greenberg, Optically switchable thin films: a review, Thin Solid Films 251 (1994) 81–93, https://doi.org/10.1016/0040-6090(94)90668-8.

[16] G.H.S. Schmid, J. Bauer, A. Eder, C. Eisenmenger-Sittner, A hybrid hydrolytic hydrogen storage system based on catalyst-coated hollow glass microspheres, Int. J. Energy Res. 41 (2017) 297–314, https://doi.org/10.1002/er.3659.

[17] X. Qi, C. Gao, Z. Zhang, S. Chen, B. Li, S. Wei, Fabrication and characterization of millimeter-sized glass shells for inertial confinement fusion targets, Chem. Eng. Res. Des. 91 (2013) 2497–2508, https://doi.org/10.1016/j.cherd.2013.03.010.

[18] E. Pérez, M. González, C. Cienfuegos, E. Chávez, D. Ruíz, J. Pinto, S. Gutiérrez, M. García, Design of an electric vehicle accumulator with LiFePO4 batteries for green transportation, in: 2021 IEEE Mexican Humanitarian Technology Conference (MHTC), 2021, pp. 31–37.

[19] J.M. Gonzalez-Gonzalez, S. Martin, P. Lopez, J.A. Aguado, Hybrid battery-ultracapacitor storage system sizing for renewable energy network integration, IET Renew. Power Gener. 14 (2020) 2367–2375, https://doi.org/10.1049/iet-rpg.2019.1310.

[20] T. Li, X.-Z. Yuan, L. Zhang, D. Song, K. Shi, C. Bock, Degradation mechanisms and mitigation strategies of nickel-rich NMC-based lithium-ion batteries, Electrochem. Energy Rev. 3 (2020) 43–80, https://doi.org/10.1007/s41918-019-00053-3.

[21] J. Xu, F. Lin, M.M. Doeff, W. Tong, A review of Ni-based layered oxides for rechargeable Li-ion batteries, J. Mater. Chem. A 5 (2017) 874–901, https://doi.org/10.1039/C6TA07991A.

[22] S.-M. Bak, E. Hu, Y. Zhou, X. Yu, S.D. Senanayake, S.-J. Cho, K.-B. Kim, K.Y. Chung, X.-Q. Yang, K.-W. Nam, Structural changes and thermal stability of charged LiNixMnyCozO2 cathode materials studied by combined in situ time-resolved XRD and mass spectroscopy, ACS Appl. Mater. Interfaces 6 (2014) 22594–22601, https://doi.org/10.1021/am506712c.

[23] X. Cui, L. Ai, L. Mao, Y. Xie, Y. Liang, N. Zhang, Y. Feng, S. Wang, S. Li, Enhanced electrochemical properties of LiNi0.6Co0.2Mn0.2O2 cathode material by the diffusional Al2O3 coating layer, Ionics 25 (2019) 411–419, https://doi.org/10.1007/s11581-018-2725-x.

[24] S.-H. Lee, G.-J. Park, S.-J. Sim, B.-S. Jin, H.-S. Kim, Improved electrochemical performances of LiNi0.8Co0.1Mn0.1O2 cathode via SiO2 coating, J. Alloys Compd. 791 (2019) 193–199, https://doi.org/10.1016/j.jallcom.2019.03.308.

[25] W. Zhang, L. Liang, F. Zhao, Y. Liu, L. Hou, C. Yuan, Ni-rich LiNi0·8Co0·1Mn0·1O2 coated with Li-ion conductive Li3PO4 as competitive cathodes for high-energy-density lithium ion batteries, Electrochim. Acta 340 (2020) 135871, https://doi.org/10.1016/j.electacta.2020.135871.

[26] Z. Peng, G. Yang, F. Li, Z. Zhu, Z. Liu, Improving the cathode properties of Ni-rich LiNi0.6Co0.2Mn0.2O2 at high voltages under 5 C by Li2SiO3 coating and Si4+ doping, J. Alloys Compd. 762 (2018) 827–834, https://doi.org/10.1016/j.jallcom.2018.05.226.

[27] M. Horkel, H. Mahr, J. Hell, C. Eisenmenger-Sittner, E. Neubauer, Determination of the thickness of metal coatings on granular diamond materials by spatially resolved optical methods, Vacuum 84 (2009) 57–60, https://doi.org/10.1016/j.vacuum.2009.04.010.

[28] J.A. Johnson, J.L. Priedeman, G.B. Thompson, Influence of mechanical agitation on the conformal coating of powders, Surf. Coat. Technol. 453 (2023) 129131, https://doi.org/10.1016/j.surfcoat.2022.129131.

[29] M. Ghislandi, E. Tkalya, B. Marinho, C.E. Koning, G. de With, Electrical conductivities of carbon powder nanofillers and their latex-based polymer composites, Composites, Part A, Appl. Sci. Manuf. 53 (2013) 145–151, https://doi.org/10.1016/j.compositesa.2013.06.008.

[30] J.M. Montes, F.G. Cuevas, J. Cintas, J.M. Gallardo, Electrical conductivity of metal powder aggregates and sintered compacts, J. Mater. Sci. 51 (2016) 822–835, https://doi.org/10.1007/s10853-015-9405-2.

[31] E.M. Lee, H.L. Clack, Powder resistivity inferred differential collection of heterogeneous coal fly ash and powered activated carbon admixtures within a cylindrical electrostatic precipitator, Emiss. Control Sci. Technol. 2 (2015) 33–43, https://doi.org/10.1007/s40825-015-0029-4.

[32] T.J. Garino, Electrical behavior of oxidized metal powders during and after compaction, J. Mater. Res. 17 (2002) 2691–2697, https://doi.org/10.1557/jmr.2002.0389.

[33] 3M™, Glass bubbles S38, http://multimedia.3m.com/mws/media/694361O/3m-glass-bubbles-s38.pdf. (Accessed 5 April 2023).

[34] Targray, Targray NMC powder for battery manufacturers, https://www.targray.com/li-ion-battery/cathode-materials/nmc. (Accessed 5 April 2023).

[35] MSE Supplies, Lithium nickel manganese cobalt oxide, LiNi0.8Co0.1Mn0.1O2 NMC 811 cathode powder, https://www.msesupplies.com/collections/cathode-materials/products/lithium-nickel-manganese-cobalt-oxide-lini0-8co0-1mn0-1o2-nmc-811-cathode-powder-500g?variant=39840355647546. (Accessed 5 April 2023).

[36] C.A. Schneider, W.S. Rasband, K.W. Eliceiri, NIH image to ImageJ: 25 years of image analysis, Nat. Methods 9 (June 2012) 671–675, https://doi.org/10.1038/nmeth.2089.

[37] M. Zogg, Einführung in die Mechanische Verfahrenstechnik, Teubner Verlag, 1993.

[38] G.H.S. Schmid, C. Eisenmenger-Sittner, J. Hell, M. Quirchmair, Vorrichtung zum Beschichten eines Substrats, Patent AT 513 037 B1 2014-01-15, TU Wien, 2014.

[39] H. Mahr, Optische Schichtdickenbestimmung auf granularen Materialien, Ph.D. thesis, TU Wien, 2023.

[40] D. Depla, S. Mahieu (Eds.), Reactive Sputter Deposition, Springer, Berlin, Heidelberg, 2008.

[41] R. Kurinjimala, D. Böhm, W. Pessenhofer, C. Eisenmenger-Sittner, Physical vapor deposited coatings on high Ni content NMC811 Li-ion battery cathode powder, Surf. Coat. Technol. 462 (2023) 129472, https://doi.org/10.1016/j.surfcoat.2023.129472.

[42] R. Heckel, An analysis of powder compaction phenomena, Trans. Metall. Soc. AIME 221 (1961) 1001–1008.

[43] R. Heckel, Density-pressure relationship in powder compaction, Trans. Metall. Soc. AIME 221 (1961) 671–675.

[44] A. Bunde, W. Dieterich, Percolation in composites, J. Electroceram. 5 (2000) 81–92, https://doi.org/10.1023/a:1009997800513.

[45] A. Bunde, J.W. Kantelhardt, Diffusion and conduction in percolation systems, in: P. Heitjans, J. Kärger (Eds.), Diffusion in Condensed Matter, 2 ed., Springer-Verlag, 2005, pp. 895–914.

[46] S.-R. Jian, G.-J. Chen, W.-M. Hsu, Mechanical properties of Cu2O thin films by nanoindentation, Materials 6 (2013) 4505–4513, https://doi.org/10.3390/ma6104505.

[47] K. Zeng, K. Breder, D.J. Rowcliffe, C. Herrström, Elastic modulus determined by hertzian indentation, J. Mater. Sci. 27 (1992) 3789–3792, https://doi.org/10.1007/bf00545457.